Available online at www.sciencedirect.com
SCIENCE DIRECT
Biomaterials 27 (2006) 4399–4408
Biomaterials
www.elsevier.com/locate/biomaterials

Porogen-based solid freeform fabrication of polycaprolactone–calcium phosphate scaffolds for tissue engineering

Mark J. Mondrinos[a], Robert Dembzynski[b], Lin Lu[b], Venkata K.C. Byrapogu[b], David M. Wootton[b], Peter I. Lelkes[a,*], Jack Zhou[b]

[a]*School of Biomedical Engineering, Science and Health Systems, Drexel University, Philadelphia, PA, USA*
[b]*Department of Mechanical Engineering and Mechanics, Drexel University, Philadelphia, PA, USA*

Received 5 November 2005; accepted 21 March 2006
Available online 5 May 2006

Abstract

Drop on demand printing (DDP) is a solid freeform fabrication (SFF) technique capable of generating microscale physical features required for tissue engineering scaffolds. Here, we report results toward the development of a reproducible manufacturing process for tissue engineering scaffolds based on injectable porogens fabricated by DDP. Thermoplastic porogens were designed using Pro/Engineer and fabricated with a commercially available DDP machine. Scaffolds composed of either pure polycaprolactone (PCL) or homogeneous composites of PCL and calcium phosphate (CaP, 10% or 20% w/w) were subsequently fabricated by injection molding of molten polymer-ceramic composites, followed by porogen dissolution with ethanol. Scaffold pore sizes, as small as 200 μm, were attainable using the indirect (porogen-based) method. Scaffold structure and porosity were analyzed by scanning electron microscopy (SEM) and microcomputed tomography, respectively. We characterized the compressive strength of 90:10 and 80:20 PCL–CaP composite materials (19.5 ± 1.4 and 24.8 ± 1.3 Mpa, respectively) according to ASTM standards, as well as pure PCL scaffolds (2.77 ± 0.26 MPa) fabricated using our process. Human embryonic palatal mesenchymal (HEPM) cells attached and proliferated on all scaffolds, as evidenced by fluorescent nuclear staining with Hoechst 33258 and the Alamar Blue™ assay, with increased proliferation observed on 80:20 PCL–CaP scaffolds. SEM revealed multilayer assembly of HEPM cells on 80:20 PCL–CaP composite, but not pure PCL, scaffolds. In summary, we have developed an SFF-based injection molding process for the fabrication of PCL and PCL–CaP scaffolds that display in vitro cytocompatibility and suitable mechanical properties for hard tissue repair.

Keywords: Calcium phosphate; Polycaprolactone; Composite; Scaffold; Mechanical properties; Cell proliferation

1. Introduction

Tissue engineering is an interdisciplinary field that draws from materials science, cell biology, and biotechnology to synthesize effective strategies for repair or replacement of damaged or diseased tissues [1]. Typically, in vitro bone tissue engineering uses engineered 3-D scaffolds [2] made of synthetic biodegradable polymers [3] or bioceramics [4], as substrates for 3-D culture of osteoblasts or other applicable cell types. The recent application of solid freeform fabrication (SFF) to manufacturing scaffolds for tissue engineering [5–8] is limited by the fact that SFF machines must be adapted to the fluid mechanical properties of each biomaterial under consideration. For drop-on-demand-printing (DDP) and fused deposition modeling, the machine parameters must match the physical properties of the build material, such as viscosity and surface tension. These properties vary greatly amongst different biomaterials, precluding the use of a single machine for direct fabrication of scaffolds from multiple biomaterials, requiring more complicated multi-nozzle designs. Therefore, it is desirable

Abbreviations: Au, gold; CAD, computer-aided design; CaP, calcium phosphate; CM, compressive modulus; DDP, drop-on-demand printing; FBS, fetal bovine serum; HEPM, human embryonic palatal mesenchyme; MEM, minimum essential medium; PBS, phosphate buffered saline; PCL, polycaprolactone; Pd, palladium; SEM, scanning electron microscopy; SFF, solid freeform fabrication; UCS, ultimate compressive strength; μCT, micro computed tomography; SD, standard deviation

*Corresponding author. Tel.: +1 215 895 2219; fax: +1 215 895 4983.
E-mail address: pilelkes@drexel.edu (P.I. Lelkes).

0142-9612/$ - see front matter © 2006 Elsevier Ltd. All rights reserved.
doi:10.1016/j.biomaterials.2006.03.049

to develop SFF fabrication processes in which a single, universal porogen material is used to build porogens that may then be injected with a wide range of biomaterials.

The innate rigidity of the synthetic biodegradable polymer polycaprolactone (PCL) makes this material well suited for the fabrication of tissue engineering scaffolds, mainly for orthopedic applications [9,10]. Calcium phosphate (CaP), a major constituent of native extracellular matrix in bone [11], is frequently used as a scaffold material for bone tissue engineering [12–14]. In the past, we designed and implemented a thermoplastic porogen-based process for the fabrication of cytocompatible injection molded CaP cement (CPC) scaffolds [15]. In extending these studies, we now used two well-defined biomaterials, PCL and CaP, to generate cytocompatible composite scaffolds with precise architectural features and appropriate mechanical properties for hard tissue repair by injection molding of thermoplastic porogens fabricated by DDP.

2. Materials and methods

2.1. Drop-on-demand printing machine

All thermoplastic porogens were fabricated using a commercial DDP machine (Solidscape™ ModelMaker II, Merrimack, NH) based on thermoplastic ink jetting technology (Fig. 1). Porogens were built based on a simplified CAD model generated using Pro/Engineer™ (Fig. 2).

2.2. Structured porogen design

The Pro/Engineer™-designed injectable porogen model with 100% interconnectivity is shown in Fig. 2. Each void of the square scaffold is in the shape of a cube and is separated from adjacent voids by struts on four of its sides. Scaffold porogens were designed with discrete pore sizes varying between 200 and 600 μm. In order to empirically determine the minimum porogen basin wall thickness and maximum biomaterial injection temperature for which thermoplastic porogens would consistently maintain structural integrity, simple destructive testing was conducted. Based on these preliminary experiments, a 3.18 mm wall thickness and a biomaterial injection temperature of 75 °C were selected.

In order to minimize air entrapment and weld line formation, the porogen was designed such that molten biomaterial would flow into the cavities of the porogen through a single gate or injection port (Fig. 2B). The dimensions of the port's cross-section were equal to the pore size of the particular scaffold being injected (e.g. the gate was $600 \times 600\,\mu m^2$ for 600 μm-wide pores), except for the fabrication of 200 μm pore scaffolds, which required an opening of $250 \times 250\,\mu m^2$. Therefore, a transition region was needed to go from a relatively large basin where molten material could be deposited down to the gate dimension corresponding to the desired pore size of the scaffold being fabricated (Fig. 2B). The interior diameter of the basin was designed such that the plunger of a standard plastic 1 ml syringe could be used to force the molten biomaterial into the cavities of the porogen (Fig. 2A). A cutout view model of the desired resultant scaffold geometry following porogen injection and subsequent removal is shown in Fig. 2C.

2.3. Fabrication of scaffolds

Following fabrication of structured thermoplastic porogens, scaffolds were generated by injection molding as described below.

PCL Scaffolds: PCL pellets (average molecular weight = 65,000, Sigma) were melted in an oven (VWR 1410) at 75 °C. Concomitantly, the porogens were also preheated to 75 °C. Molten PCL was drawn into a

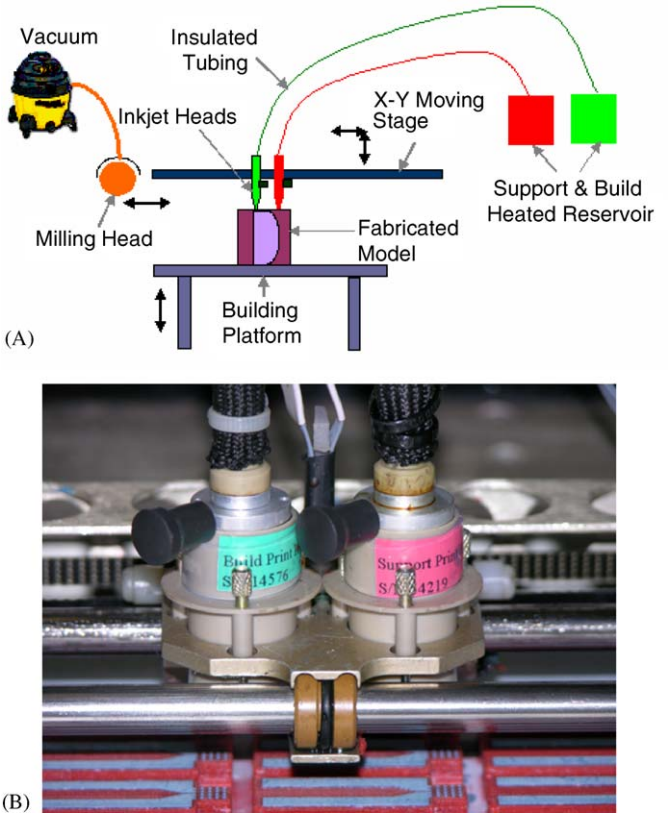

Fig. 1. Drop-on-demand three dimensional printing system: (A) diagram of drop-on-demand (DDP) system components; (B) digital photograph of inkjet print heads in this DDP system, Solidscape Modelmaker II.

1 ml syringe. The flat tip of the syringe was placed into the basin, thus allowing the plunger of the syringe to advance from the syringe body into the cylindrical basin of the porogen (Fig. 2A). The syringe was emptied quickly and the filled porogen was allowed to cool to room temperature. After solidifying, excess PCL which had extruded out of the openings on the sides of the porogen and the porogen basin was trimmed.

In order to separate the porogen from the scaffold structure after biomaterial solidification, the filled porogens were immersed into 99% ethanol (Fisher) in a 10 ml test tube. The tubes were shaken vigorously and the solvent replaced every 15–20 s, until all (colored) porogen material was dissolved, as evaluated by the colorless appearance of the solvent. Using this method, most of the porogen material was removed in <5 min, with soaking for no more than 1 h to remove residual thermoplastic from the scaffold center. After porogen removal, the scaffolds were then allowed to air-dry at room temperature and stored dry as long as needed prior to cell culture and mechanical testing.

PCL–CaP composite scaffolds: PCL–CaP composite scaffolds were fabricated in the same fashion as the PCL scaffolds, after first preparing the mixture of PCL and CaP. For that, dry PCL pellets and CaP powders were weighed and mixed at the desired ratios in an aluminum specimen dish. After melting the mixture at 75 °C, the PCL–CaP was homogenized using an ultrasonic probe, and reheated as necessary; total mixing time was approximately 30 min. Scaffolds were made with ratios (w/w) of 90% PCL to 10% CaP and 80% PCL to 20% CaP.

2.4. Microcomputed tomography

Nine scaffolds with 600 μm pores made of pure PCL, 90:10 and 80:20 PCL–CaP ($n = 3$ for each material) were fabricated and scanned using a SkyScan 1072 Microtomograph (μCT) scanner (Micro Photonics). This is a compact, desktop X-ray system for non-destructive 3-D microscopy with 5 μm resolution and 2 μm detectability operating at 100 kV, yielding

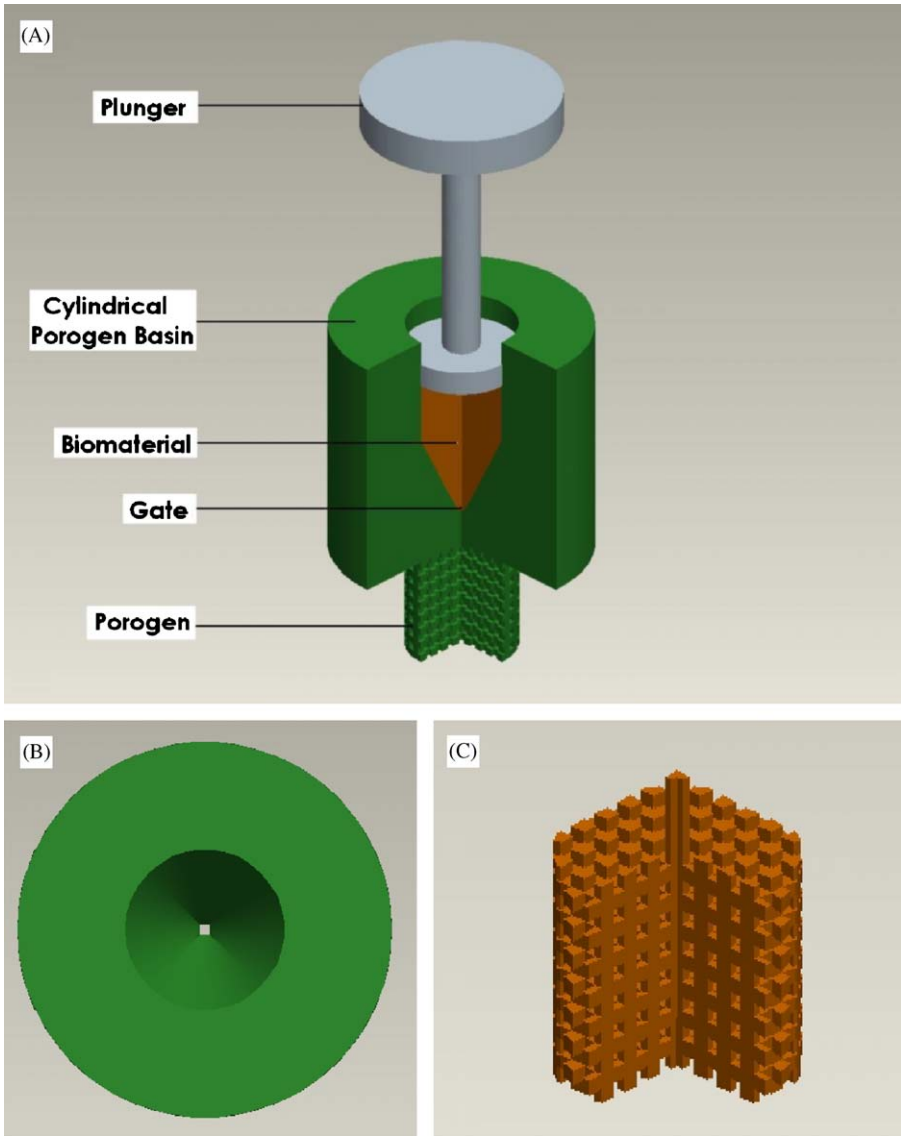

Fig. 2. Computer generated models (A–C) of the scaffold porogen illustrating key features of the injection molding process: (A) injectable porogen with cylindrical basin for loading molten biomaterial that is injected through the single injection gate using a syringe plunger; (B) overhead view shows the single injection gate equal to the largest sized feature in the porogen (250, 300, 400 or 600 μm^2); (C) theoretical model of resultant scaffold consisting of pores with the void volume corresponding to the porogen gate dimension (200–600 μm), cut-out view.

transmission images which can be used to reconstruct cross sections or the complete 3-D internal microstructure. The image pixel size was set at 6.1 μm in this study. The output format for each specimen was 976 serial 1024×1024 bitmap images. These slice images were viewed in SkyScan's TView software and reconstructed by CT Analyser software. By selecting darker thresholds, the struts of a specimen may be reconstructed. Conversely, by selecting the white levels of the bitmap images, the pores in the specimen can be visualized. Thresholds of the gray scale images were inverted to allow measurement of the volume of all pore spaces. The ratio of pore volume to total volume was then calculated to determine the porosity. Similarly, the contribution of void space to the strut volume was determined by calculating the ratio of strut internal void volume to total strut volume.

2.5. Scanning electron microscopy

Porogens and scaffold structures were prepared for characterization by scanning electron microscopy (SEM) according to standard protocol [16]. Briefly, non-biological samples (porogens and empty scaffolds) were air-dried and sputter coated with Au/Pd for a period of 60–120 s depending on sample architecture. Biological samples (cell-seeded scaffolds) were fixed in 2.5% aqueous gluteraldehyde for 1 h at room temperature then overnight at 4 °C, dehydrated through graded alcohols, dried with a critical point dryer (SPI supplies). Samples were then examined with a scanning electron microscope (SEM, XL-30 Environmental SEM-FEG or Amray 1830 SEM), both using an acceleration voltage of 10.0 kV.

2.6. Mechanical testing

Compression tests of solid cylinders made of PCL and PCL–CaP were performed on an Instron 5543 uniaxial testing system using a 1 kN load cell. Five specimens of each material were tested according to the guidelines specified in ASTM D695-02a [17]. In addition, compression testing was done on 600 μm pore pure PCL scaffolds ($n = 6$) at a compression rate of 1 mm/min using the same system described

above with a 100 N load cell. Effective stress was computed based on the macroscopic scaffold cross-sectional area. The ultimate compressive strength (UCS) as well as the compression modulus (CM) was calculated from the effective stress–strain diagrams, as previously described [17].

2.7. Cell culture

The cytocompatibility of the scaffolds was assessed using human embryonic palatal mesenchymal (HEPM) cells (American Type Culture Collection, ATCC, CRL-1486). These cells are routinely maintained in Eagles' minimum essential medium (MEM) with Earles' salts supplemented with 10% fetal bovine serum (Hyclone), 2.0 mM L-glutamine, 1.0 mM sodium pyruvate, 0.1 mM non-essential amino acids, and 1.5 g/l sodium bicarbonate at 37 °C in a 5% CO_2 incubator [16].

For cell culture studies, the scaffolds were sterilized with 70% ethanol for 1 h at room temperature, and washed 3 × 5 min with sterile phosphate buffered saline (PBS). The scaffolds were then incubated with a mixture of 30 μg/ml collagen type I (BD Biosciences) and Matrigel™ (BD Biosciences, diluted 1:30) in MEM for 1 h at 37 °C to facilitate extracellular matrix protein adsorption and enhanced cellular attachment. Scaffolds were then seeded with a suspension of 1 million HEPM cells/ml overnight on an orbital shaker (Belly Dancer, Stovall). Following seeding, scaffolds were transferred to 24-well plates, allowed to equilibrate for 2 h in the described cell culture medium and the initial level of cell seeding was assessed by the Alamar Blue (AB, Biosource) assay [16]. In order to assess cell proliferation on the various scaffolds the AB assay was performed again on the same samples at day 4 post-seeding. Subsequently, the samples were fixed in 10% buffered formalin (Fisher) for 1 h at room temperature and stored in PBS at 4 °C until cytological staining. For staining, the samples were washed once more with PBS and incubated with PBS containing 2 μg/ml Hoechst 33258 (Bisbenzimide, Sigma), a nuclear stain.

2.8. Statistical analysis

All data are presented as means ± standard deviation (SD). The number of samples analyzed is listed for each experiment, except for the cell culture experiment, where the number of samples for each scaffold was 5. Statistical significance of Alamar Blue™ measurements was assessed by one way ANOVA with Tukey-Cramer post-tests for multiple comparisons, defining $p<0.05$ as significant. Due to unequal variance, comparisons for the compressive testing were performed with one-tailed t-test followed by the Welch correction for significantly different standard deviations.

3. Results and discussion

3.1. Scaffold fabrication

In previous studies, generation of biocompatible scaffolds using injectable porogens has been accomplished by polymer solution casting [6]. However, most of the solvents which are commonly used to solubilize synthetic biopolymers, such as dimethyl formamide, chloroform, and dioxane, are highly cytotoxic and will also dissolve the proprietary thermoplastic material used with the Solidscape™ machine, making solution casting difficult to implement in our process. Therefore, in order to use the parts fabricated by the machine without any secondary processing, we chose to inject molten biopolymers into the porogen.

Thermoplastic porogens (Fig. 2), which were designed as described in Section 2, were used to generate PCL and PCL–CaP composite scaffolds by injection molding of molten polymer. Porogens designed with 600, 400 and 250 μm pore sizes, yielded PCL and PCL–CaP composite scaffolds with nominal pore sizes of 600, 400, and ~200 μm, respectively. μCT analysis based views of an 80:20 PCL–CaP composite scaffold fabricated using a 600 μm porogen are shown in Fig. 3. Pore corners in the horizontal build plane (x–y directions) were quite sharp (Fig. 3A and B), whereas rounding of the scaffold pore corners was observed in the vertical build plane (z-axis, Fig. 3C).

The porosity of our 600 μm scaffolds was determined for each of the materials by volumetric analysis of 3-D reconstructions from μCT data (see Fig. 3). For the 600 μm scaffolds, the theoretical porosity based on the porogen design was 59.9%, while measured values were 52.6% for pure PCL, 57.2% and 58.2% for 90:10 and 80:20 PCL–CaP composites, respectively. These data conform fairly well (within <5% for 90:10 and 80:20 PCL–CaP) to the theoretically calculated porosity. The somewhat higher porosities observed for the PCL–CaP composites vs. pure PCL may be due to resistance to flow within the porogen

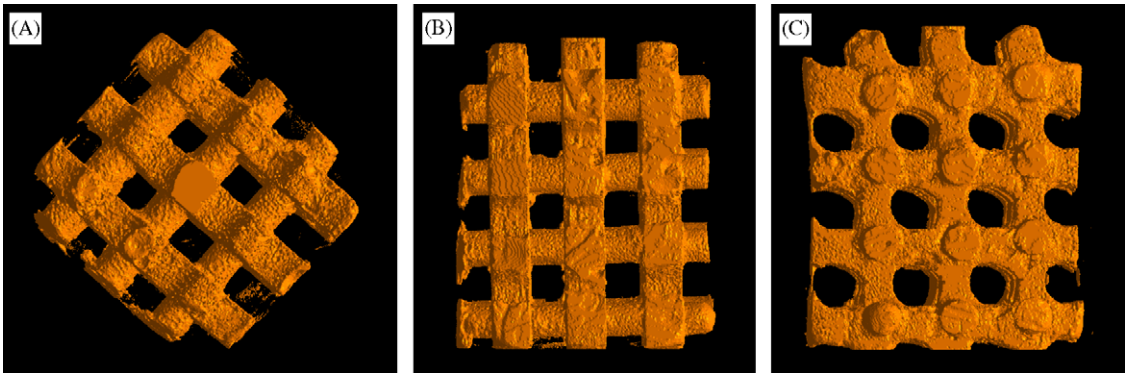

Fig. 3. Microcomputed tomography analysis of 80:20 PCL–CaP composite scaffolds: (A) view of horizontal build plane (looking down the longest dimension), note the sharp square pores; (B) view of horizontal build plane (looking down shortest dimension), note the sharp square pores; (C) view of vertical build plane, note the rounded pores.

caused by the solid CaP particles, whereas the pure PCL melt flows more freely during injection molding, thus more completely filling and compressing the porogen.

The microporous architecture of fabricated scaffolds, and in some cases thermoplastic porogens, was further assessed by SEM as described in Section 2 (Fig. 4). An SEM micrograph of a 400 μm thermoplastic porogen and an 80:20 PCL–CaP composite scaffold fabricated using a 600 μm porogen are shown in Fig. 4A and B, respectively. The measured pore sizes of our scaffolds, as evaluated from SEM micrographs, conformed well to the predicted sizes, based on the designs of the porogens. The measured pore sizes of pure PCL scaffolds fabricated using 400 and 600 μm thermoplastic porogens were 396 ± 40 μm ($n = 6$) and 607 ± 12 μm ($n = 6$). In attempting to reproducibly fabricate PCL scaffolds with 200 μm^2 pore diameters, we found that porogens with pore diameters of ~250 μm yielded scaffolds with rectangular shaped pores with an average pore size of 198 ± 38 μm ($n = 3$) (Fig. 4C). An example of these pores is shown at higher magnification in Fig. 4D. When using 250 μm porogens, the porogens either did not completely fill or we obtained scaffolds with irregular-shaped pores in the regions that maintained any structural integrity, indicating the current limitations of this scaffold manufacturing process.

We note that other SFF systems have been able to generate structures with features of 200 μm or less using direct building methods with PCL [18–20]. For example, using a solution casting approach, Vozzi et al. [20] developed a microsyringe deposition system capable of depositing 2-D lines with widths as low as 20 μm using a 2.5% poly L-lactic acid (PLLA)/20% PCL solution. However, the manufacturing process reported by these authors was limited by the fact that it did not allow for the effective fabrication of macroscopic 3-D scaffolds. The pore sizes in our scaffolds are comparable with some of the highest resolution SFF systems capable of fabricating 3-D macroscopic scaffolds reported in the literature. For example, Geng et al. [5] reported pore sizes of 200–500 μm using a direct printing system with the polysaccharide chitosan. Darling and Sun [18] used precision extrusion deposition of computer-aided design (CAD) models to fabricate PCL scaffolds with pore sizes and strut widths of 200–300 μm. Similarly, Zein et al. [19]

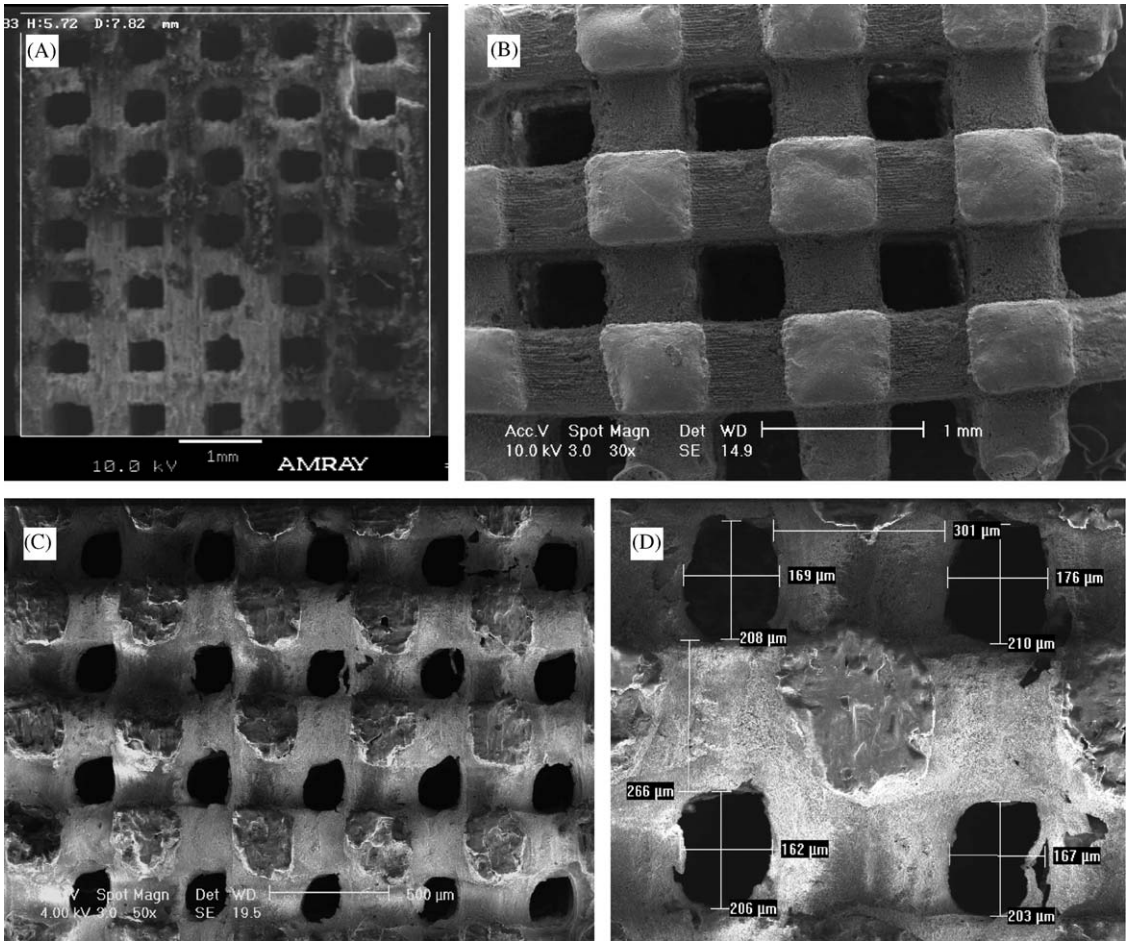

Fig. 4. Scanning electron microscopy of representative thermoplastic porogen and scaffolds: (A) thermoplastic porogen used for fabrication of 400 μm PCL and PCL–CaP scaffolds; (B) 80:20 PCL–CaP composite scaffold fabricated using 600 μm porogen; (C) PCL scaffold fabricated from 250 μm porogen; (D) high magnification SEM micrograph of PCL scaffold fabricated from 250 μm porogen, example pore size measurements used for quantification are shown. Magnification and/or scale bar indicated in images.

used fused depostion modeling to fabricate PCL scaffolds with struts of 260–370 μm in diameter and pore sizes of 160–700 μm, which is similar to the smallest pore sizes seen in our scaffolds (Fig. 4D). All direct build SFF methods cited above are limited by the fact that the manufacturing process must be re-configured for each material used. By contrast, our approach is more versatile; the machine must be configured only once for the ubiquitous porogen which may then be filled with any biomaterial having a melting temperature below 75 °C.

Taboas et al. [6] used an indirect thermoplastic porogen approach comparable to our process. However, their process is complicated by the fact that an additional step of casting ceramic into the thermoplastic is required. Thus, upon dissolution of the thermoplastic, Taboas et al. injection-molded poly lactic acid (PLA) into the ceramic to generate scaffolds with macropore sizes of 500 μm and an internal microporous structure on the order of 50–100 μm produced by salt leaching. Our process, which intrinsically is simpler than that of Taboas et al., is easily amenable to the introduction of salt leaching approaches; it would require an additional leaching step in aqueous medium following thermoplastic porogen removal.

3.2. Mechanical testing

To test the mechanical properties of PCL–CaP composites we performed compression testing as described in Section 2. As seen in Fig. 5 the increase in CaP content of the composite significantly raised the compressive modulus (CM) and UCS of the samples ($p<0.002$). In order to assess potential mechanical effects of the porogen leaching and sterilization by EtOH, we conducted preliminary mechanical tests of cylinders soaked in EtOH for 5 days. While specimen integrity was not affected by EtOH exposure, we noted a reduction in the CM and ultimate compression strength (data not shown). These preliminary results suggest that care should be taken to minimize EtOH exposure time during scaffold manufacture. Current experiments are underway to clarify this issue in more detail.

In addition to testing the mechanical properties of solid cylinders made of the diverse scaffold materials, we tested the compressive strength of pure PCL scaffolds with 600 μm pore size. Scaffold stress–strain curves show multiple failure points due to failure of the weakest strut, prior to collapse of the entire scaffold structure (Fig. 6). Pure PCL scaffolds had UCS values of 2.77 ± 0.26 MPa and a CM of 44.0 ± 3.2 MPa. The UCS value is in line with reported values for trabecular bone from human mandibles ranging from 0.22 to 10.44 MPa [21]. We note that the compressive strength of trabecular bone varies greatly with anatomical location and individual factors such as bone density, volume fraction of the sample being measured, and strain rate [22]. Our scaffolds are considerably less stiff than and hence not suitable for replacing cortical bone, for which UCS values of over 200 MPa have

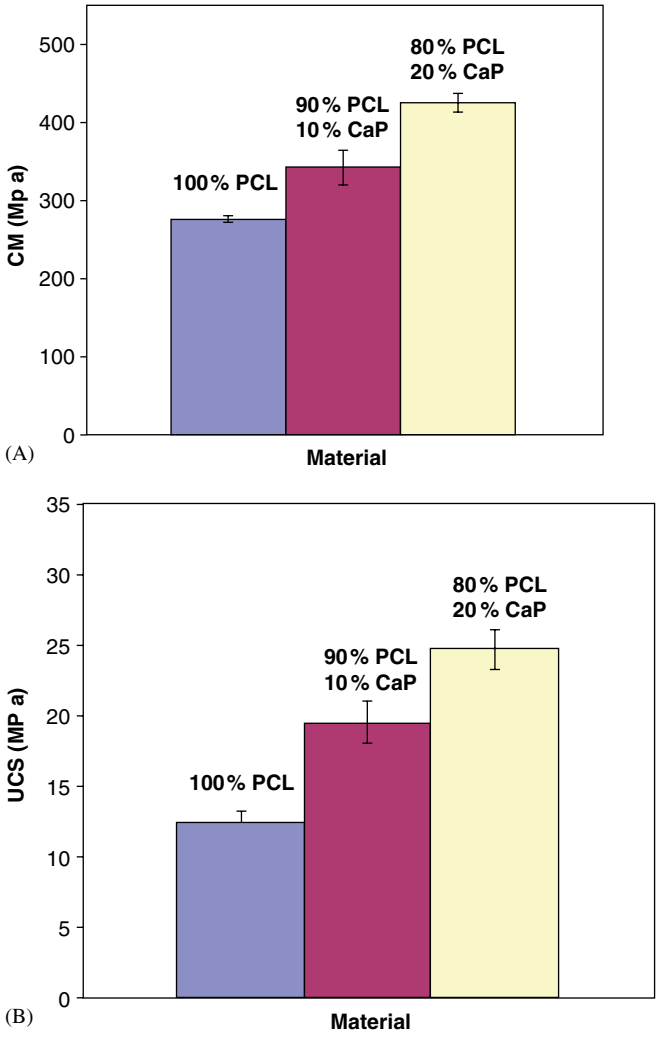

Fig. 5. Compressive mechanical properties of PCL–CaP composites: (A) comparison of the CM of 100% PCL, 90:10 and 80:20 PCL–CaP cylinders; (B) comparison of the UCS with different concentrations of CaP. Bars represent mean ± standard deviation. Statistical analysis indicate that the material properties are significantly different ($p<0.002$, t-test, one-tail: assuming unequal variances) for different concentrations of CaP.

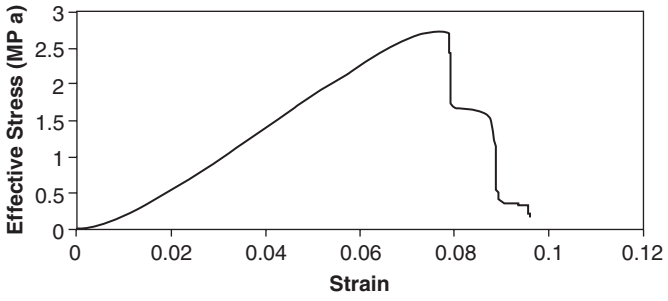

Fig. 6. Typical stress–strain curve for a 600 μm 100% PCL scaffold. Multiple failures seen in the figure are due to the failure of weakest strut among the struts.

been reported [22]. The small standard deviation (<10% coefficient of variation) for CM and UCS of the solid cylinders as well as 100% PCL scaffolds demonstrates the reproducibility of the mechanical properties achieved using this process.

An important issue related to measured mechanical properties of our scaffolds is the presence of voids in the struts resulting from the injection molding process. Microcomputed tomography (μCT) analysis indicated that for pure PCL scaffolds only 0.06% of the strut volume was contributed by voids, whereas the value rose to 0.77% in the case of 80:20 PCL–CaP scaffolds, presumably due to mixing artifacts in the slurry-like, particle-containing polymer melt. We therefore conclude that the mechanical properties of our scaffolds are not adversely affected by inclusion of excessive voids. The mechanical test results can be compared to scaffold mechanical properties reported by others for PCL scaffolds of similar porosity (Table 1). CM was slightly higher than Hutmacher et al. [23], in the range reported by Zein et al. [19], and slightly lower than reported by Williams et al. [7]. UCS is essentially equal to 0.2% offset yield stress in our experiments, due to the brittle failure mode of most samples. The mean UCS of our scaffolds was at the high end of the reported range for PCL scaffold yield stress in the literature [7,19,23].

3.3. Cell-biomaterial interactions

The cytocompatibility of PCL and PCL–CaP composite 3-D scaffolds was assessed using the Alamar Blue™ assay for cell metabolic activity/cell proliferation as described in Section 2. HEPM cells growing on the scaffolds were visualized by fluorescent staining of cell nuclei, and SEM. Previously, we demonstrated that HEPM cells seeded onto the surface of thermoplastic-molded solid disks of CPC attached and proliferated similarly to culture on the "gold standard" TCPS, indicating no significant limitations in cellular function due to potential residual thermoplastic components [15]. In the case of 3-D scaffolds of PCL and 80:20 PCL–CaP, HEPM cells were able to attach as evidenced by fluorescent nuclear staining with Hoechst 33258 (Fig. 7). These images indicate attachment onto the struts of both PCL (Fig. 7A) and 80:20 PCL–CaP composite scaffolds (Fig. 7B). Based on the Alamar Blue™ data, the initial seeding efficacy was not significantly different for the materials used (data not shown). This similar level of HEPM cell attachment to all materials used was probably due to the fact that all scaffolds were pre-coated with a mixture of Matrigel™, a reconstituted extracellular matrix, and collagen type I solution. Without this coating, cellular attachment to the synthetic surfaces was minimal only (data not shown).

Once attached, HEPM cells proliferated on all types of 3D scaffolds, as assessed from the Alamar Blue™ fluorescence data (Fig. 8), with some differences between materials. The normalized cell proliferation data indicated an identical cell proliferation on pure PCL and 90:10 PCL–CaP scaffolds. By contrast, cell growth on the 80:20 scaffolds was significantly enhanced ($p<0.05$). The AB data was corroborated qualitatively by the observed increase in the density of Hoechst 33258–stained nuclei following 4 days of post-seeding culture in vitro on the various scaffolds (Fig. 9). We note that at this time point, cells were visibly growing both on the struts (Figs. 9A and C), as well as in the interior pore structures of all scaffolds investigated (Figs. 9B and D). For further confirmation of cellular ingrowth into the scaffold center, the scaffolds were cut into segments using a scalpel. The presence of cells on all interior surfaces was visualized by nuclear staining (Fig. 9E).

The morphology of HEPM cells growing on PCL and 80:20 PCL–CaP composite scaffolds was assessed by SEM. As seen in Fig. 10A the cells flattened on the rather smooth PCL surface. By contrast, on the 80:20 PCL–CaP the cells seemed to form multilayer assemblies (Fig. 10B), which further corroborates the increased density of nuclear staining (Figs. 7 and 9) and significantly higher level of cell proliferation (Fig. 8) as compared to 100% PCL. In summary, these cytocompatibility tests clearly indicate that all porogen-based scaffolds when coated with suitable ECM proteins facilitate attachment and support proliferation of HEPM cells in vitro. In addition, our data suggest that the presence of CaP in the PCL–CaP composite enhances the proliferation of HEPM cells and reduces their spreading in favor of multi-layer assembly.

Table 1
Porosity and compressive mechanical properties of PCL scaffolds fabricated by various SFF techniques

	Porosity (%)	Compressive strength or yield stress (MPa)	Compressive modulus (MPa)
Hutmacher et al. [23][a]	61.1	2.0–3.1	21.5–41.9
Zein et al. [19][b]	48–77	0.4–3.6	4–77
Williams et al. [7][b]	63–79	2.0–3.2	52–67
This study	52.5	2.77±0.26	44±3.2

[a]Range of mechanical properties reported reflects differences between two strut lay-down patterns (constant porosity) in either dry condition or wet in saline.

[b]Range of mechanical properties reported reflects the dependence on porosity, in both cases the compressive mechanical properties increased with decreasing porosity.

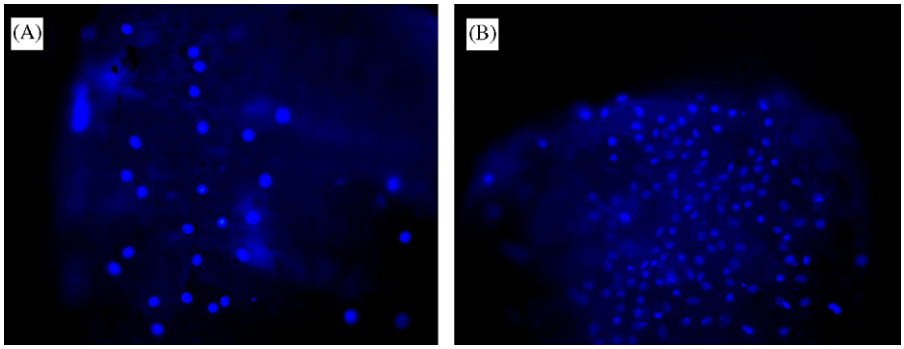

Fig. 7. Bisbenzimide nuclear staining of adherent HEPM cells following 24 h of orbital shaker seeding on PCL (Panel A, 200 ×) and 80:20 PCL–CaP composite (Panel B, 100 ×) scaffolds, 600 μm pore sizes. Images are captured by imaging the surface of a strut on the outside of the scaffold.

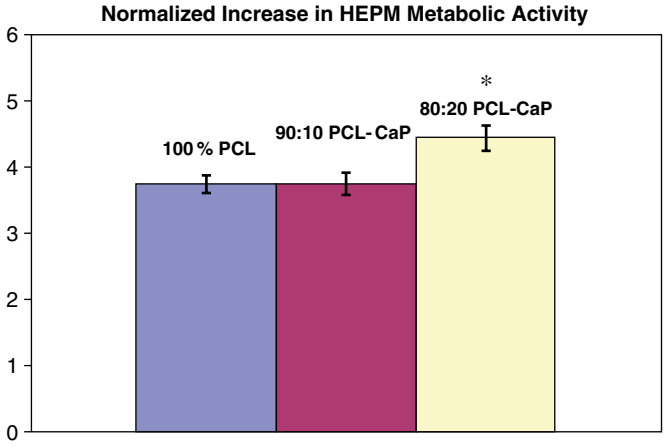

Fig. 8. Normalized increase in Alamar Blue™ readings over the 4-day in vitro culture period following the initial 24 h seeding period for 600 μm pore size pure PCL, 90:10 and 80:20 PCL–CaP scaffolds. Metabolic activity as measured by Alamar Blue™ at 96 h post-seeding was normalized to the Alamar Blue™ readings taken immediately following the 24 h seeding period. Y-error bars represent the standard deviation from the mean for each sample ($n = 5$). * = Statistically significant differences ($p < 0.05$) compared to 100% PCL by one-way ANOVA with Tukey–Cramer post-tests for multiple comparisons.

Our findings are in line with previous reports showing that PCL scaffolds fabricated using various manufacturing processes display good cytocompatibility in vitro [18,23] and are biocompatible in vivo [7]. For example, Williams et al. [7] used selective laser sintering (SLS) to fabricate PCL scaffolds which were then seeded with human gingival fibroblasts genetically modified to express bone morphogenetic protein-7 (BMP-7) and implanted into subcutaneous pockets of immunocompromised mice. These scaffolds supported the development of new bone over a 4-week period, as evidenced by μCT detection of mineralized tissue [7]. Darling and Sun [18] reported that precision extrusion-deposited PCL scaffolds supported the proliferation of cultured rat cardiomyoblasts, however detailed analysis of cellular metabolism, proliferation, and morphology were not provided. Hutmacher et al. [23] used primary human fibroblasts and human osteoprogenitor cells to demonstrate the biocompatibility of PCL scaffolds fabricated by fused deposition modeling, although the capacity of these scaffolds to induce bone formation was not addressed.

Diverse scaffolds fabricated from CaP and diverse CaP composites also display in vitro [24,25] and in vivo [26] biocompatibility. For example, Wang et al. [24] demonstrated that biomimetic nano-structured CaP scaffolds, fabricated by gel lamination technology, supported osteogenic differentiation, as evidenced by alkaline phosphatase expression. Xu et al. [25] used a murine osteoblast cell line to demonstrate biocompatibility of CaP–chitosan composites with amorphous architecture and pore sizes of 165–270 μm. These scaffolds were fabricated by preparing a water-soluble mannitol—CaP–chitosan mixture and subsequent removal of mannitol to create the pore structure. Amorphous poly(lactic-*co*-glycolic acid) PLGA–CaP scaffolds of various weight ratios, fabricated by admixing PLGA microparticles into Ca-P cement and implanted into subcutaneous and cranial defects in rats, facilitated fibrovascular and bone tissue development over a 12-week period, respectively [26]. Compared to these amorphous CaP scaffolds, the primary advantage of SFF scaffolds is that they are comprised of precisely generated structures which allow for reproducible scaffold fabrication and control of mechanical properties.

4. Conclusion

In this paper, we established a thermoplastic porogen-based injection molding manufacturing process and demonstrated efficient, reproducible fabrication of porous PCL and PCL–CaP composite scaffolds with pore sizes as small as 200 μm. With their interconnected porous structure, these scaffolds will be suitable for specific tissue engineering applications, such as replacement of trabecular bone, etc. In vitro cytocompatibility has been demonstrated for both our PCL and PCL–CaP scaffolds. The primary advantage of these porogen-based process is the ability to use multiple biomaterials for injection molding with a single ubiquitous

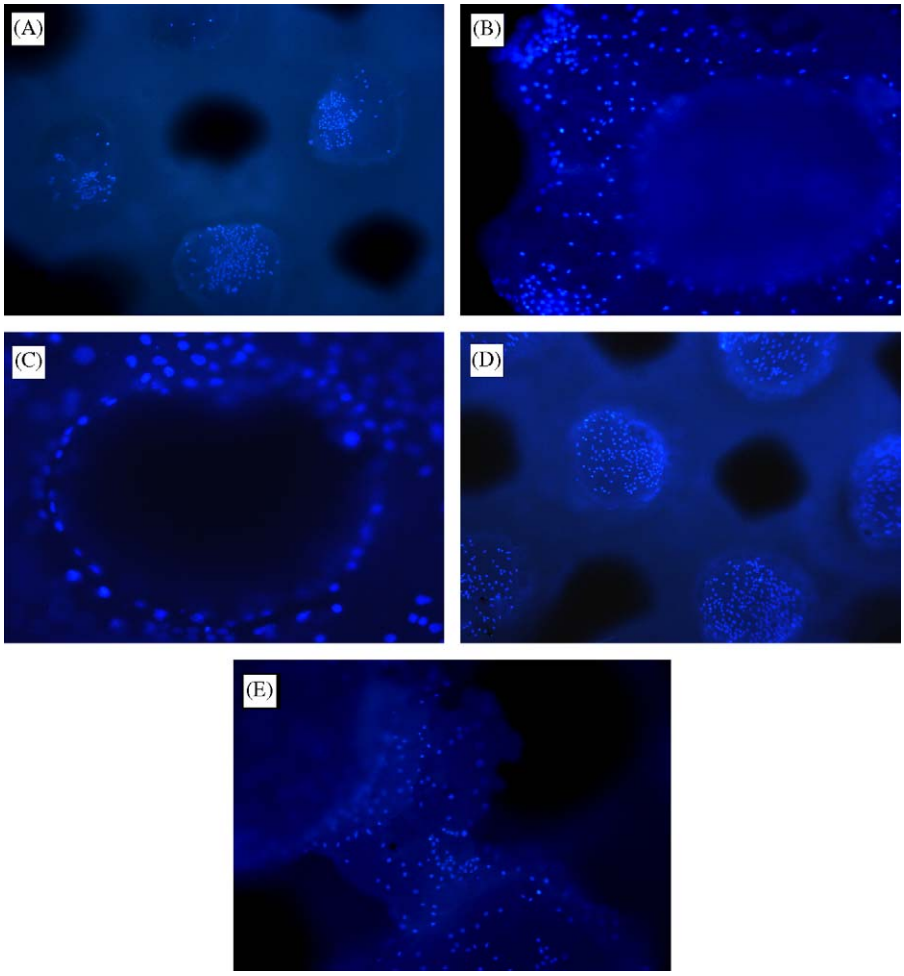

Fig. 9. Bisbenzimide staining of HEPM cells cultured on PCL (Panels A and B) and 80:20 PCL–CaP composite (Panels C and D) scaffolds for 5 days: (A) HEPM cells on the surface struts of a 600 μm pore size PCL scaffold (50 ×); (B) HEPM cells growing around and into a pore on the same scaffold imaged in panel A (100 ×); (C) HEPM cells on the surface struts of a 600 μm pore size 80:20 PCL–CaP composite scaffold (50 ×), note the increased density of nuclear staining relative to the PCL scaffold; (D) HEPM cells colonizing a pore in the scaffold imaged in panel C (original magnification 200 ×); (E) HEPM cells growing on a strut from the scaffold center (100 ×).

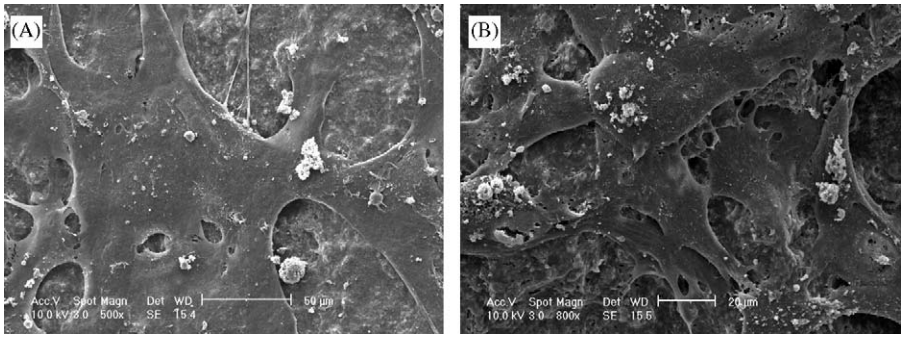

Fig. 10. Scanning electron micrographs of HEPM cells cultured on 600 μm pore size PCL and 80:20 PCL–CaP scaffolds for 5 days: (A) flattened HEPM cells on PCL scaffold, scale bar = 50 μm; (B) multilayered HEPM cells on 80:20 PCL–CaP scaffold, scale bar = 20 μm.

porogen. As an added advantage, the indirect porogen technique can improve the resolution of our 3-D SFF system by at least 2-fold as compared to directly built scaffolds. Current work in our laboratory focuses on optimizing the mechanical properties of our composite PCL–CaP scaffolds and investigating the ability to generate mineralized bone tissue constructs in vitro using optimized scaffolds seeded with mesenchymal stem cells.

Acknowledgments

We gratefully acknowledge the support by the National Science Foundation (NSF, DMI-0300405) and thank the Machine Shop of Drexel University for helping us to make some machine parts. We thank Dr. Mengyan Li for her assistance with SEM.

References

[1] Langer R, Vacanti J. Tissue engineering. Science 1993;260:920–6.
[2] Mistry AS, Mikos AG. Tissue engineering strategies for bone regeneration. Adv Biochem Eng Biotechnol 2005;94:1–22.
[3] Thomson RC, Mikos AG, Beahm E, Lemon JC, Satterfield WC, Aufdemorte TB, et al. Guided tissue fabrication from periosteum using preformed biodegradable polymer scaffolds. Biomaterials 1999;20(21):2007–18.
[4] Ohgushi H, Miyake J, Tateishi T. Mesenchymal stem cells and bioceramics: strategies to regenerate the skeleton. Novartis Found Symp 2003;249:118–27 (discussion 127–32, 170–4, 239–41).
[5] Geng L, Feng W, Hutmacher DW, Wong YS, Loh HT, Fuh JYH. Direct writing of chitosan scaffolds using a robotic system. Rapid Prototyping J 2005;11(2):90–7.
[6] Taboas JM, Maddox RD, Krebsbach PH, Hollister SJ. Indirect solid free form fabrication of local and global porous, biomimetic and composite 3D polymer-ceramic scaffolds. Biomaterials 2003;24(1):181–94.
[7] Williams JM, Adewunmi A, Schek RM, Flanagan CL, Krebsbach PH, Feinberg SE, et al. Bone tissue engineering using polycaprolactone scaffolds fabricated via selective laser sintering. Biomaterials 2005;26(23):4817–27.
[8] Hollister SJ, Maddox RD, Taboas JM. Optimal design and fabrication of scaffolds to mimic tissue properties and satisfy biological constraints. Biomaterials 2002;23(20):4095–103.
[9] Shin M, Yoshimoto H, Vacanti JP. In vivo bone tissue engineering using mesenchymal stem cells on a novel electrospun nanofibrous scaffold. Tissue Eng 2004;10(1–2):33–41.
[10] Rohner D, Hutmacher DW, Cheng TK, Oberholzer M, Hammer M. In vivo efficacy of bone-marrow-coated polycaprolactone scaffolds for the reconstruction of orbital defects in the pig. J Biomed Mater Res 2003;66B(2):574–80.
[11] Wilt FH. Developmental biology meets materials science: morphogenesis of biomineralized structures. Dev Biol 2005;280(1):15–25.
[12] Ruhe PQ, Hedberg EL, Padron NT, Spauwen PH, Jansen JA, Mikos AG. rhBMP-2 release from injectable poly(DL-lactic-*co*-glycolic acid)/calcium-phosphate cement composites. J Bone Joint Surg Am 2003;85-A(Suppl 3):75–81.
[13] Xu HH, Quinn JB, Takagi S, Chow LC. Synergistic reinforcement of in situ hardening calcium phosphate composite scaffold for bone tissue engineering. Biomaterials 2004;25(6):1029–37.
[14] Barralet JE, Grover L, Gaunt T, Wright AJ, Gibson IR. Preparation of macroporous calcium phosphate cement tissue engineering scaffold. Biomaterials 2002;23(15):3063–72.
[15] Lu L, Dembzynski RS, Mondrinos MJ, Wootton D, Lelkes PI, Zhou J. Manufacturing system development for fabrication of bone scaffolds. In: Proceeding of ASME IMECE 2005, International mechanical engineering congress and exposition, Orlando, Florida, November 5–11, 2005.
[16] Li M, Mondrinos MJ, Gandhi MR, Ko FK, Weiss AS, Lelkes PI. Electrospun protein fibers as matrices for tissue engineering. Biomaterials 2005;26(30):5999–6008.
[17] Wang F, Shor L, Darling A, Khalil S, Sun W, Guceri S, et al. Precision extruding deposition and characterization of cellular poly ε-caprolactone tissue scaffolds. Rapid Prototyping J 2004;10(1):42–9.
[18] Darling AL, Sun W. 3D microtomographic characterization of precision extruded poly epsilon-caprolactone scaffolds. J Biomed Mater Res 2004;70B(2):311–7.
[19] Zein I, Hutmacher DW, Tan KC, Teoh SH. Fused deposition modeling of novel scaffold architectures for tissue engineering applications. Biomaterials 2002;23(4):1169–85.
[20] Vozzi G, Previti A, De Rossi D, Ahluwalia A. Microsyringe-based deposition of two-dimensional and three-dimensional polymer scaffolds with a well-defined geometry for application to tissue engineering. Tissue Eng 2002;8(6):1089–98.
[21] Misch CE, Qu Z, Bidez MW. Mechanical properties of trabecular bone in the human mandible: implications for dental implant treatment planning and surgical placement. J Oral Maxillofac Surg 1999;57(6):700–6 (discussion 706–8).
[22] Carter DR, Hayes WC. Bone compressive strength: the influence of density and strain rate. Science 1976;194:1174–6.
[23] Hutmacher DW, Schantz T, Zein I, Ng KW, Teoh SH, Tan KC. Mechanical properties and cell cultural response of polycaprolactone scaffolds designed and fabricated via fused deposition modeling. J Biomed Mater Res 2001;55(2):203–16.
[24] Wang T, Tian WD, Liu L, Cheng XZ, Liao YM, Li SW. The study of cell biocompatibility of new pattern biphasic calcium phosphate nanocomposite in vitro. Hua Xi Kou Qiang Yi Xue Za Zhi 2005;23(2):106–9.
[25] Xu HH, Simon Jr CG. Fast setting calcium phosphate-chitosan scaffold: mechanical properties and biocompatibility. Biomaterials 2005;26(12):1337–48.
[26] Ruhe PQ, Hedberg EL, Padron NT, Spauwen PH, Jansen JA, Mikos AG. Biocompatibility and degradation of poly(DL-lactic-*co*-glycolic acid)/calcium phosphate cement composites. J Biomed Mater Res 2005;74(4):533–44.